ARMA 20–XXXX

SAND2020-1783C

Subsurface airflow measurements before and after a small chemical explosion

Bauer, S.J., S.T. Broome

Sandia National Laboratories, Albuquerque, NM, USA,

Gardner, W.P.

University of Montana, Missoula USA,

This paper was prepared for presentation at the 54th US Rock Mechanics / Geomechanics Symposium held in Golden, Colorado, USA, 17–20 June 2020. This paper was selected for presentation at the symposium by an ARMA Technical Program Committee based on a technical and critical review of the paper by a minimum of two technical reviewers. The material, as presented, does not necessarily reflect any position of ARMA, its officers, or members. Electronic reproduction, distribution, or storage of any part of this paper for commercial purposes without the written consent of ARMA is prohibited. Permission to reproduce in print is restricted to an abstract of not more than 200 words; illustrations may not be copied. The abstract must contain conspicuous acknowledgement of where and by whom the paper was presented.

ABSTRACT:

To increase understanding of damage associated with underground explosions, a field test program was developed jointly by Sandia and Pacific Northwest National Laboratories at the EMRTC test range in Socorro, NM. The Blue Canyon Dome test site is underlain by a rhyolite that is fractured in places. The test system included deployment of a defined array of Geoprobe® soil vapor implants at specific depths (~4-5.5m vertical spacing to a depth of ~60m) and lateral spacings (~4.6 and ~7.6m) from a central borehole in eight near vertical boreholes. The monitoring boreholes radially surround a central near vertical shot hole in cardinal and 45 degrees offset to cardinal directions. The probes are potted in coarse sand which touches/accesses the rhyolite. The probes are individually accessed via nylon tubing and isolated from each other by epoxy and grout sequences.

Pre and post chemical explosion air flow measurements near each gas probe were observed for potential change. The gas flow measurement is a function of the rock mass permeability near a probe. A diaphragm pump was used to pump air from each zone for ~30-45 minutes. Gas flow measurements were made at each probe before and after the detonation. Much of the flow rate change is at depth station 8 (59.4m) and is in the SE quadrant. Flow rate changes are inferred to be caused by the chemical explosion which may have opened pre-existing fractures, fractured the rock and/or caused block displacements by rotations and translations.

1. INTRODUCTION

The work presented herein is part of a test program to understand subsurface damage associated with underground chemical explosions. Within this test program, additional multi-phenomenological measurements were made (e.g. [1]), and more are in the process of being documented. The multi-measurement approach was taken to better capture and characterize the pre and post explosive condition of the rock.

The work presented in this paper focuses on relative changes in local rock permeability from before and after the explosion. Measurements before the explosion are intended to characterize the gas (air) flow conditions at each of the test stations; measurements after the explosion will help us elucidate our understanding of subsurface damage resultant of the chemical explosion.

The test site is located at the Energetic Materials Research and Testing Center (EMRTC) at the New Mexico Institute of Mining and Technology in Socorro, New Mexico. Specifically, the site sits upon Blue Canyon Dome west of Socorro NM (Figure 1). The "dome" is a three-sided promontory; the in-situ stress state is unknown.

The site is generally "dry", excepting rainwater, however during the testing processes, a large volume of water was introduced downhole into the shot hole to ensure it was full during the explosion.

The host rock at Blue Canyon Dome is the rhyolitic lava(s) of Cook Spring [2]. Our thin section and SEM observations are consistent with this classification; the rock is either a rhyolitic lava flow or a tuff deposit in which the original shards recrystallized so completely that there are no relict shard boundaries left behind. Observations supporting this classification include 1) no evidence of glass shards in the finer-grained matrix, from optical and scanning electron microscopy observations, there is, 2) no evidence of flattening within the matrix or the relict pumice (if tuff there would have been no overlying load after deposition to cause flattening), 3) the micropores and mineral-filled fractures could be found in either a lava flow or a densely welded tuff.

The rhyolitic lava is a Cenozoic ~30mya banded rhyolite (Figure 2) from the Datil group [3], locally intermittently fractured with small vugs (Figure 2). The rhyolite is aphanitic and from quantitative X-ray diffraction, composed of quartz (55 %), and sanidine (45 %), the high

temperature form of potassium feldspar with a general formula K(AlSi3O8).

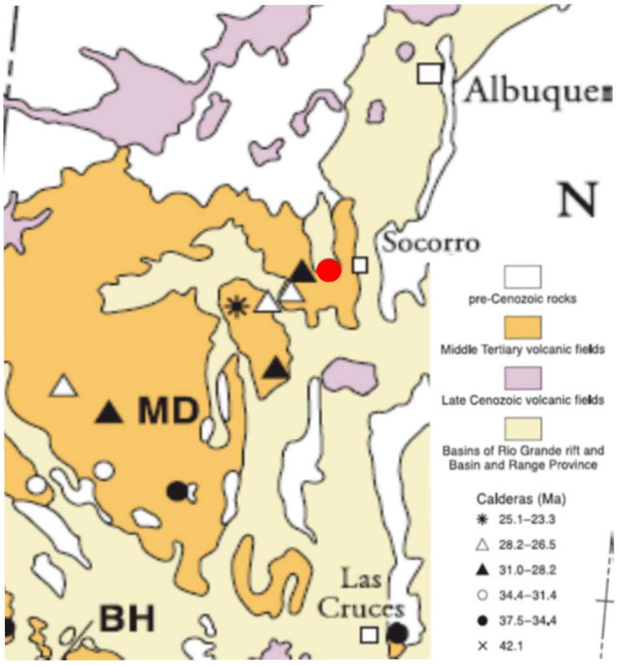

Figure 1. Location map from [2]. Red dot is approximate location of the field site.

Figure 2. Field exposures of flow banded rhyolite (A) with fractures (B) (near field of view ~2 meters).

2. FIELD-TEST SYSTEM AND SETUP

The test system included deployment [1] of a defined array of 128 Geoprobe® soil vapor implants at specific depths (~4-5.5m vertical spacing to a depth of ~60m) and lateral spacings (~4.6 and ~7.6m) in eight near vertical hammer-drilled 0.1524m-diameter boreholes (Figure 3). Unless otherwise stated, all depths reported are below ground surface. The monitoring boreholes surround radially a central near vertical hammer-drilled shot hole and are in cardinal (closer to the shot hole) and 45 degrees offset to cardinal directions.

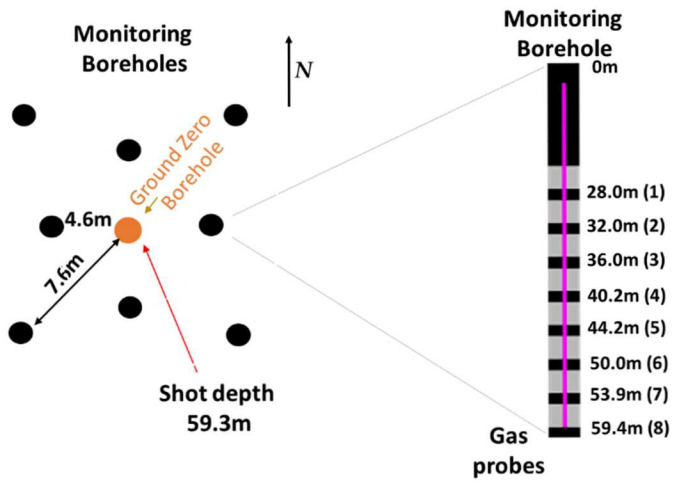

Figure 3. Sketch (not to scale): Left: Bird's eye view of monitoring bore hole array, and Right: Gas probe depths [after: 4].

The 64 soil vapor probes (Geoprobe®), are potted in coarse "playground" sand which provides a highly porous and permeable path from probe to the rhyolite-host borehole (Figure 4). The probes are individually accessed via nylon tubing plumbed to surface fittings via Swagelok™ fittings. Down-going tubes were finished with a simple screen in each sand layer to allow two-way access and recirculation to each of the probe stations. The downhole end of sampling tube terminated with the 0.1525m long, 0.635cm diameter, fine mesh screen (Geoprobe®). The sampling locations are zonally isolated from each other by epoxy and grout sequences. The epoxy was placed to mitigate potential for grout seepage into the sand. The grout provided the primary vertical permeability barrier in the borehole and the grout formulation optimizes electrical properties for Electrical Resistivity Tomography (ERT) measurements [1].

Lift heights vary due to spacing of other instrumentation; sand and epoxy layers are all nominally the same from one installation to the next, however, the grout layers vary from ~4.6m to ~10.6m.

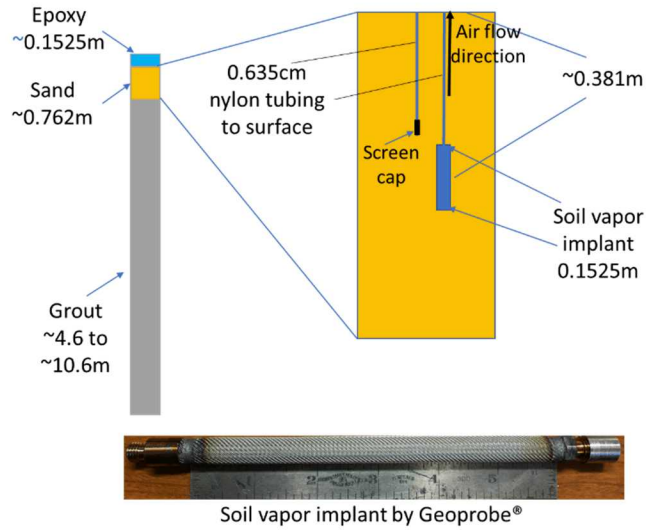

Figure 4. Image of soil vapor implant idealized deployment [2] defining sampling locations.

Using a high-flow diaphragm pump, air was pumped from each of the sample ports individually, to a manifolded array of gas flow meters (Figure 5) with flow rate ranges from 0-10 standard cubic centimeters (sccm) to 0-20 standard liters per minute (slpm). Typically flow rates began at some "greater" values and as the downhole zone was pumped down, the flow rate decreased to a "lower" value (Figure 6).

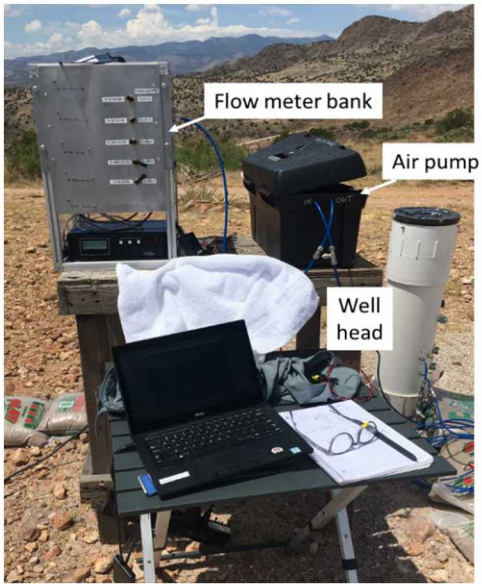

Figure 5. Field deployed flow meter bank, diaphragm pump, and well head.

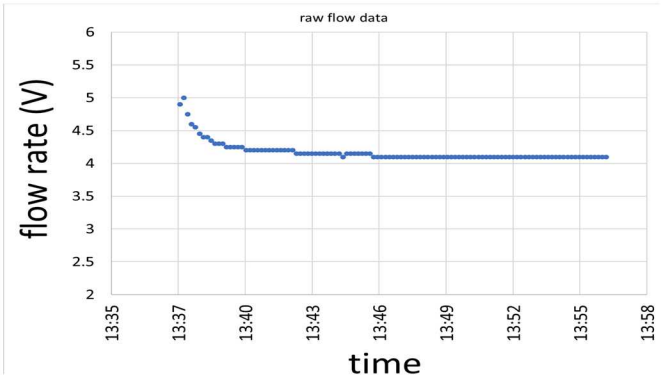

Figure 6. Example raw flow data in volts.

At each downhole sampling location, the air delivery system was connected to the upgoing tube of a discrete sampling interval housing the two nylon tubes for the potential to perform recirculation sampling. Continuity of the tubing pairs was checked for each measurement. The down-going recirculating tube was shut in with a valve, thus the sampling interval was under-pressured with respect to the surrounding reservoir during sampling. In this configuration, the induced pressure gradient caused subsurface air to advect toward the sampling locations.

Over the course of a few weeks we measured the air flow rate from the subsurface at each station. The flow rate was governed by the permeability of the rock hydraulically connected to the sand layer.

Separately, as part of our study, lab measurements were made to determine the permeability (K at 1.38 MPa confining pressure) and rudimentary mechanical properties (unconfined compressive strength [UCS], density [ρ], tensile strength [σ_T], Young's Modulus [E],

Poisson's ratio [μ]) of the rhyolite and grout were determined and are given in Table 1. The rhyolite is stiff, high strength, and its matrix of low K; whereas the grout is soft, and weak, of low K.

Table 1. Rhyolite and grout properties

	ρ (g/cc)	K* (μD)	UCS (MPa)	E (GPa)	μ	σ_T (MPa)
Rhyolite	2.40	Lab dry:~2	234	58.6	0.20	18
		Water Saturated: ~.02				
Grout	3.57	Lab dry: 100	8	2.4	0.22	2.3
		Water Saturated: ~0.1				

*apparent

3. MEASUREMENT RESULTS

Pre shot air flow rates for all stations are given in Figure 7. Notably, for the 60+ measurements there is a wide range of flow rates. Most flow rates are at or below 600 sccm, with notable exceptions.

A chemical explosive was detonated in August in the water-filled shot hole at a depth of ~59.3m. The detonation sent the explosive container into the adjacent rock, causing local rock crushing. The explosion pressurized water in the shot hole, and gas was generated during the explosion that added to the water pressurization. The results of these processes contributed to our resultant measurements.

Post shot air flow rates for all stations are given in Figure 8. Again, for the 60+ measurements there is a wide range of flow rates (a few measurement stations were not measured due to fittings damage and/or time constraints). Most flow rates are at or below 1000 sccm; there is a general increase overall. And notable exceptions of greater increases at various depths. It should be noted that in a few stations, flow rate decreased.

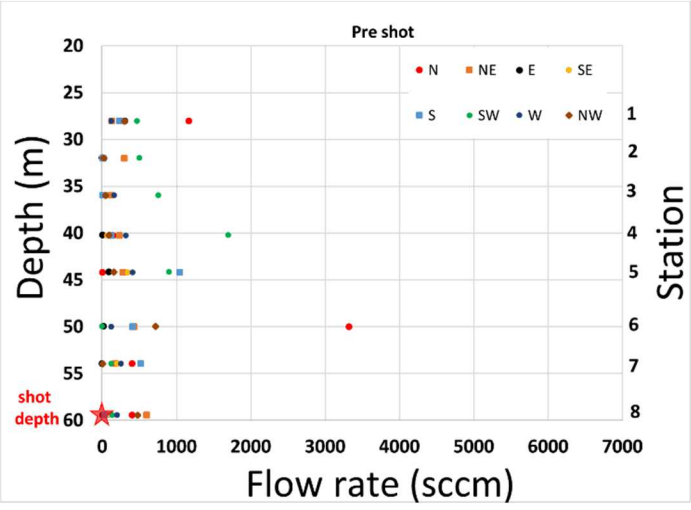

Figure 7. Measured air flow rates pre shot.

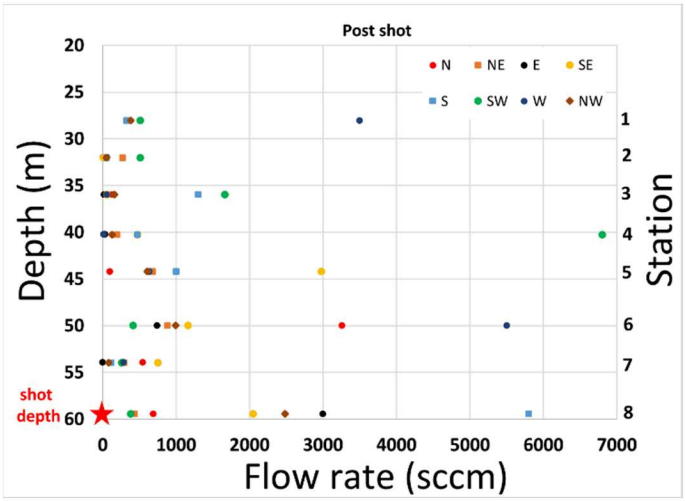

Figure 8. Measured air flow rates post shot.

Differences in flow rate for all zones recorded are plotted in map views in Figures 9 and 10 at the blue squares. Both figures have locations that are circled in red. These locations have fractures observed from pre shot borehole camera imaging within ~0.45m of the station depth. The designation of fractures in the boreholes are judgements made by reviewing the footage of all boreholes.

The most pervasive increases in flow rate are at depth 8, which is at or near the shot depth, station NE recorded a decrease. Notably, at depth 7, the pre shot flow rates are low, and remain low (small changes only) post shot, with station S exhibiting a decrease. At depth 6 there are general flow rate increases, with stations S and N exhibiting a decrease. At depth 5 the largest increase in flow rate is observed in the SW station, a fairly large increase in in the SE direction and a decrease in the S direction. At depth 4, another large increase in flow is seen the SW direction, decreases in the N, NE and W directions, and small increases in other directions. At depth 3, there are reasonable highs in the S and SW directions, decreases in the NE and W directions, and insignificant increases in other directions. At depth 2 and 1 there are mostly small changes except for a significant increase for west depth 1.

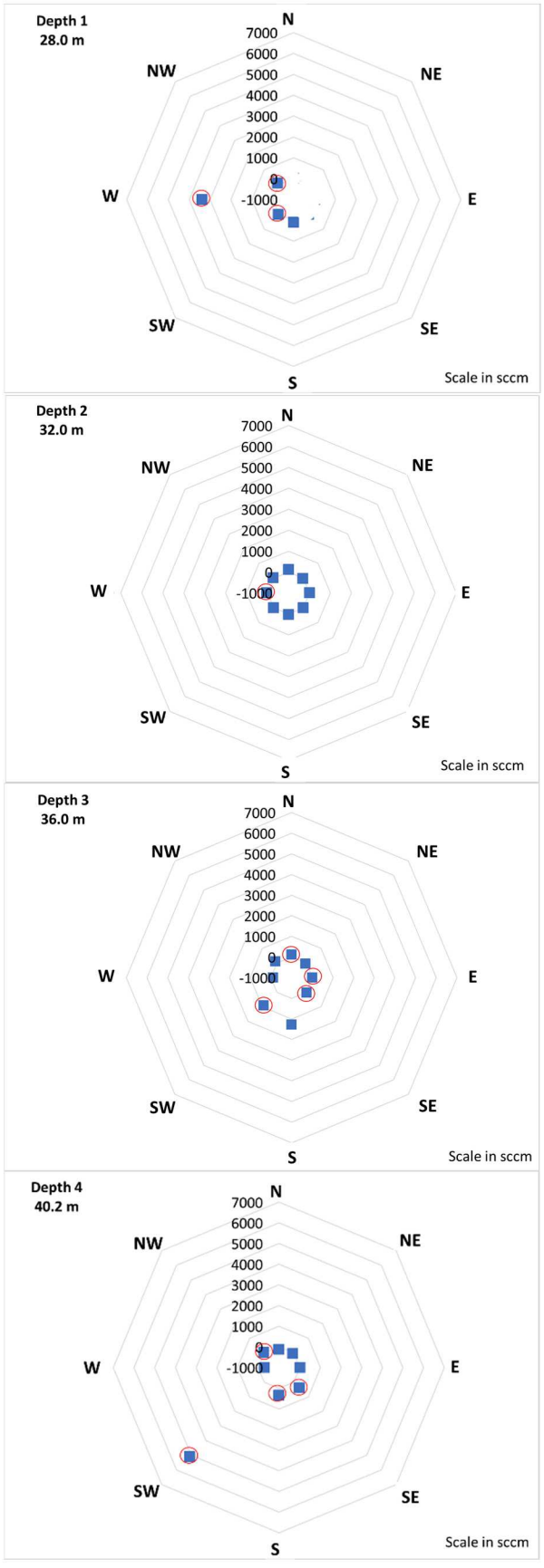

Figure 9. Post shot flow rate changes for depths 1-4. Red circles are stations fractures observed from pre shot borehole camera imaging within ~0.45m of the station depth.

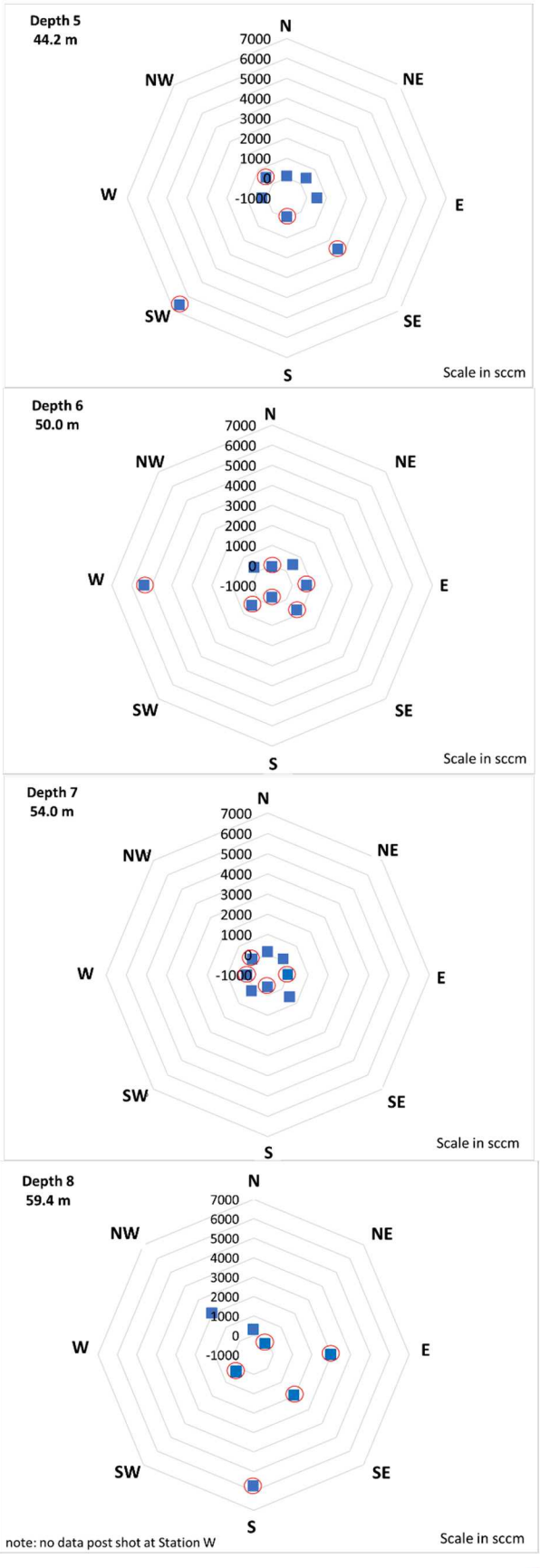

Figure 10. Post shot flow rate changes for depths 5-8. Red circles are stations fractures observed from pre shot borehole camera imaging within ~0.45m of the station depth.

4. OBSERVATIONS AND DISCUSSIONS

A few **pre shot** borehole images from monitoring boreholes are presented to demonstrate and compare flow measurements to downhole conditions and infer what happened from the shot. (The monitoring boreholes were not accessible post shot for camera viewing). In Figure 11, for North depth 6, fractures are observed in the borehole wall. This station had high pre shot flow and the same high flow rate post shot. This implies the shot did not cause a significant change to the fracture network at this fractured location. Figure 12 shows station South 5, a fractured zone with flow rate of 1000 sccm before and after the shot, again implying the shot did not cause a permeability change at this prefractured location.

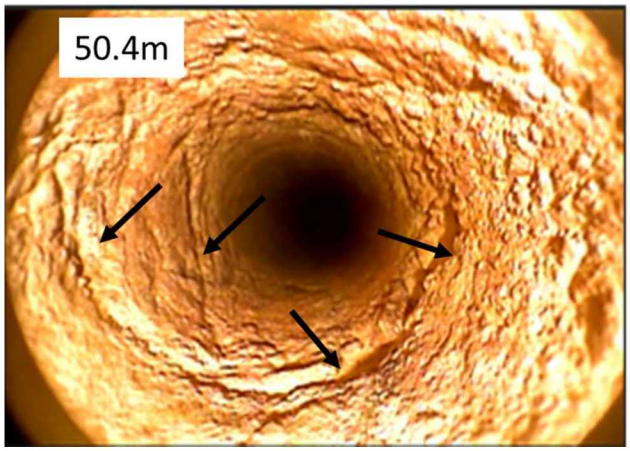

Figure 11. **Pre shot** image of north depth 6: high pre shot flow, arrows point to large fractures.

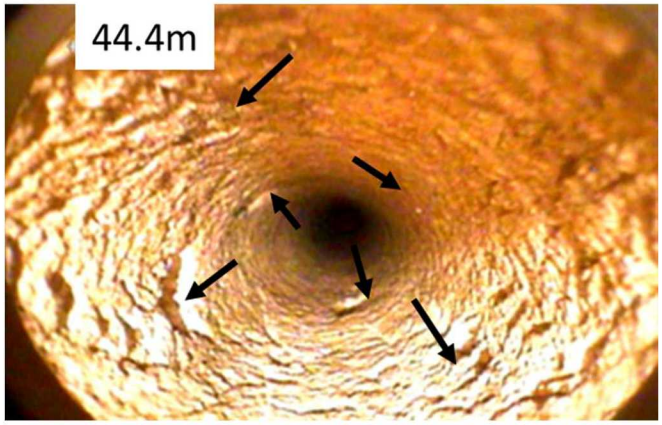

Figure 12. **Pre shot** image of south depth 5: flow rate 1000sccm pre and post shot, arrows point to fractures.

Depth 8 is at near the same depth as the explosive. In Figure 13, South depth 8 exhibits fractures; this site had low flow rate pre shot, and high flow rate post shot. This observation implies that perhaps these fractures were opened or others were created at this location. In Figure 14, East depth 8 has some visible fractures; this site had low flow rate pre shot, and high flow rate post shot. This implies that some new fractures were created or non visible fractures were opened at this location.

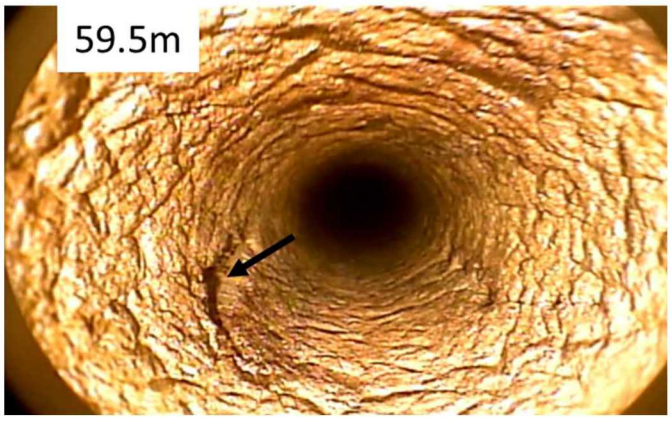

Figure 13. **Pre shot** image of south depth 8: low flow pre shot, high flow post shot.

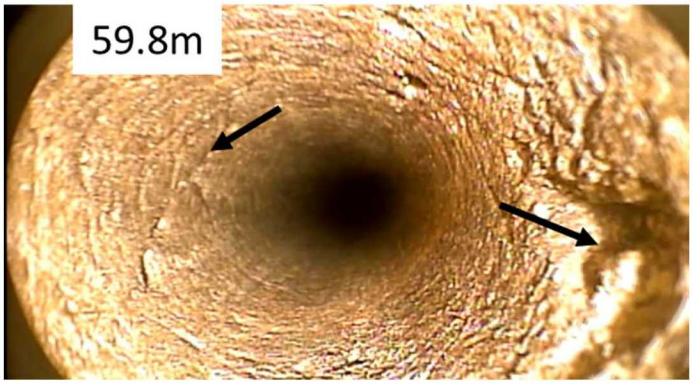

Figure 14. **Pre shot** image of east depth 8: low flow pre shot, high flow post shot.

5. DISCUSSION, SPECULATIONS, CONCLUSIONS

We have made air flow measurements at ~60 subsurface locations before and after a subsurface chemical explosion in a fractured rhyolite. Our goal has been to support characterization of the subsurface for these two conditions, and to attempt to apply the characterization to understanding the operative processes. Before the explosion, there was a wide spacial variation of flow rates observed. The pre shot flow rates may or may not correlate with observed subsurface fractures; this may be due to inability to see near wellbore fractures.

The explosive's pyro shock pressure caused near wellbore rock crushing and compaction. We observe damage to the rockmass in the form of sloughed and crushed rock (Figure 15, arrows). This image is at or near the shot location. From the increase in flow rates at depth 8 (Figure 10), it appears the damaging energy of the explosion may have extended radially in most directions.

The explosion created a shock to the rock mass. The shock could have moved and shaken the rock mass to cause some of the observed flow rate changes.

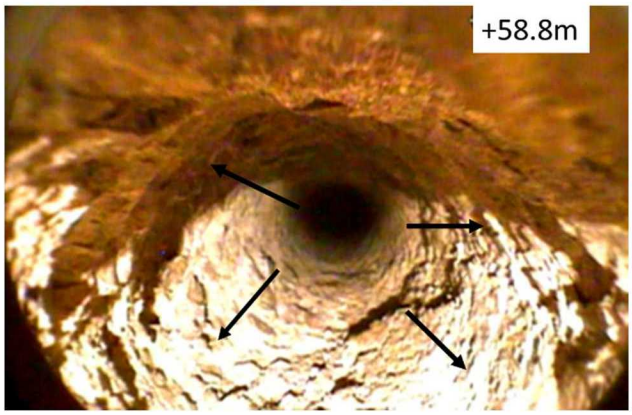

Figure 15. **Post shot** image showing crushed and fallen rock in borehole near the explosion.

The explosion created pressure to the rock (see discussion above) and to the interconnected water-filled fracture network. The explosive product gases contributed exothermally to the system, pressurizing water in the bore hole and connected fractures. The duration of the gas generation/fluid pressurization event is influential on the behavior of fracture opening and growth.

We speculate that the fluid pressurizations may have created dynamic hydraulic fractures. These fractures may look like those presented in Figure 16. There we observe numerous borehole-axial fracture about 2m above the shot where fluid pressures may have been great.

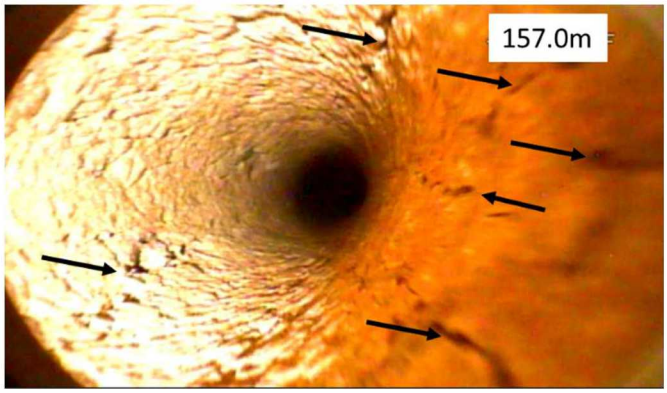

Figure 16. **Post shot** image showing dynamic hydraulic fractures on the borehole wall.

The fluids in water-saturated rock mass were dynamically pressurized by the explosion process; the interconnected fracture network was impacted in a complicated manner causing some of the flow rate changes observed.

Others [5] have used flow rate measurements and permeability determinations to estimate damage in materials. Our work only made flow measurements. We have yet to relate, much less calibrate, flow rate changes to damage. We anticipate developing this type of information to contribute to estimations of this nature.

ACKNOWLEDGEMENTS

[1] The subsurface portion of the test system design, layout and deployment was led by H. Knox and J. Knox (PNNL), and D. King, M. Ingraham and J. Feldman (SNL). P. Schwering took pre shot borehole images. J. Wilson completed the petrofabrics as part of an earlier project. The underground test system deployment was intended for test objectives not directly associated with the objectives of this paper.

[2] Figure 3 is derived from a sketch provided by M. Ingraham and project field notes.

[3] We thank D. Blankenship for his review of this paper and E. Robey for his suggestions.

The authors acknowledge the support of the National Nuclear Security Administration Office of Defense Nuclear Nonproliferation Research and Development for funding this work. This paper describes objective technical results and analysis. Any subjective views or opinions that might be expressed in the paper do not necessarily represent the views of the U.S. Department of Energy or the United States Government.

Sandia National Laboratories is a multimission laboratory managed and operated by National Technology and Engineering Solutions of Sandia, LLC., a wholly owned subsidiary of Honeywell International, Inc., for the U.S. Department of Energy's National Nuclear Security Administration under contract DE-NA-0003525.

6. REFERENCES

1. D.C. Linneman, D.P. Sprinkle, H.A. Knox, C.E. Strickland, T.C. Johnson, et al. (2019) Baseline Characterization for Change Detection with Joint Inversion of ERT and Campaign Seismic Data, AGU
2. Charles E. Chapin, Maureen Wilks, and William C. McIntosh Spacetime patterns of Late Cretaceous to present magmatism in New Mexico—comparison with Andean volcanism and potential for future volcanism, New Mexico Bureau of Geology & Mineral Resources, Bulletin 160, 2004
3. Glenn R. Osburn and Charles E. Chapin, (1983), Nomenclature for Cenozoic rocks of northeast Mogollon-Datil volcanic field, New Mexico, New Mexico Bureau of Mines
4. K. Chojnicki, (2019) personal communication.
5. V. Picandet, A. Khelidj, Bastian, G. (2001) Effect of axial compressive damage on gas permeability of ordinary and high-performance concrete Cement and Concrete Research 31 (2001) 1525–1532